Glauber dynamics of phase transitions: SU(3) lattice gauge theory

Alexei Bazavov,[1,2] Bernd A. Berg,[1,2] and Alexander Velytsky[3]
[1]*Department of Physics, Florida State University, Tallahassee, Florida 32306-4350, USA*
[2]*School of Computational Science, Florida State University, Tallahassee, Florida 32306-4120, USA*
[3]*Department of Physics and Astronomy, UCLA, Los Angeles, California 90095-1547, USA*
(Received 2 May 2006; published 5 July 2006)

Motivated by questions about the QCD deconfining phase transition, we studied in two previous papers model A (Glauber) dynamics of 2D and 3D Potts models, focusing on structure factor evolution under heating (heating in the gauge theory notation, i.e., cooling of the spin systems). In the present paper we set for 3D Potts models (Ising and 3-state) the scale of the dynamical effects by comparing to equilibrium results at first and second order phase transition temperatures, obtained by reweighting from a multicanonical ensemble. Our finding is that the dynamics entirely overwhelms the critical and noncritical equilibrium effects. In the second half of the paper we extend our results by investigating the Glauber dynamics of pure SU(3) lattice gauge on $N_\tau N_\sigma^3$ lattices directly under heating quenches from the confined into the deconfined regime. The exponential growth factors of the initial response are calculated, which give Debye screening mass estimates. The quench leads to competing vacuum domains of distinct Z_3 triality, which delay equilibration of pure gauge theory forever, while their role in full QCD remains a subtle question. As in spin systems we find for pure SU(3) gauge theory a dynamical growth of structure factors, reaching maxima which scale approximately with the volume of the system, before settling down to equilibrium. Their influence on various observables is studied and different lattice sizes are simulated to illustrate an approach to a finite volume continuum limit. Strong correlations are found during the dynamical process, but not in the deconfined phase at equilibrium.

DOI: 10.1103/PhysRevD.74.014501 PACS numbers: 05.50.+q, 11.15.Ha, 12.38.Gc, 25.75.−q

I. INTRODUCTION

In investigations of the QCD deconfining phase transition (or crossover) by means of heavy-ion experiments, one ought to be concerned about nonequilibrium effects due to the *rapid heating* of the system. With this in mind we have investigated in previous papers [1,2] the model A [3] (Glauber) dynamics of 2D and 3D Potts models. Model A dynamics includes all diffusive stochastic local updating schemes (Metropolis, heatbath, etc.) and not just the process introduced in [4]. In 3D Potts models spins provide degrees of freedom, which mimic Polyakov loops effectively [5], while in 2D, analytical results [6] allow one to check on the accuracy of the employed numerical methods. For other approaches to simulate nonequilibrium quantum fields see Ref. [7].

The QCD high temperature vacuum is characterized by ordered Polyakov loops, which are similar to spins in the low temperature phase of the 3D 3-state Potts model. We model heating by a quench from the disordered into the ordered phase, which thus corresponds to a cooling quench in the analogue spin model. Time evolution after the quench leads to vacuum domains of distinct triality under the Z_3 center of the SU(3) gauge group. It appears that these competing domains are the underlying cause for the explosive growth of structure factors $F_i(t)$, which we encounter in the time evolution after a heating quench. We use the term *spinodal decomposition* loosely to denote generically such a time period of globally unstable behavior.

Relaxation of the system at its new temperature only becomes feasible after each structure factor has overcome its maximum value. While the maximum value of the structure factor diverges with lattice size, its initial and final equilibrium values are finite in the normalization chosen in the paper. The time (measured in updates per degree of freedom) for reaching the maximum diverges with lattice size unless the underlying order-order symmetry is broken. Once the system has equilibrated at high temperature, the subsequent temperature falloff is driven by spatial lattice expansion and the system stays in quasiequilibrium during this period. So one has different time scales under heating and cooling [8].

The early time evolution of SU(3) gauge theory after the quench is well described by stochastic equations, which follow from dynamical generalizations of equilibrium Landau-Ginzburg effective action models. We calculate the exponential growth factor of this linear approximation and use a phenomenological model [9] to estimate the Debye screening mass for two temperatures above the deconfining T_c.

Finally, we compare measurements of Polyakov loop correlations, gluonic energy densities, and pressures around structure function maxima with their equilibrated values in the deconfined region at high temperatures. These measurements are of interest for a scenario in which the heating process turns back to cooling before actually reaching the equilibrium side of the structure factor maxima. In the conclusions we continue this discussion.

In the next section we introduce our notations and some preliminaries. Section III deals with Potts models. First equilibrium properties of structure functions are estab-

lished by means of multicanonical simulations of the 3D Ising and 3-state Potts model. Subsequently, their dynamical evolution after a quench is investigated, extending previous results. In Sec. IV we present our simulations of pure SU(3) lattice gauge theory. Some SU(3) data were already reported at the 2004 APS DPF conference [10]. As these simulations are very CPU time consuming it took over one more year to collect the present statistics. A summary and conclusions are given in Sec. V.

II. NOTATION AND PRELIMINARIES

We summarize our basic notations and concepts in this section.

A. Models

We simulate q-state Potts models with the energy function

$$E = 2\sum_{\langle ij\rangle}\left(\frac{1}{q} - \delta_{q_i q_j}\right) \tag{1}$$

where the sum is over nearest neighbors of a hypercubic lattice in D dimensions. The spins q_i of the system take on the values $q_i = 0, \ldots, q-1$. The factor of 2 and the term $1/q$ are introduced to match for $q = 2$ with Ising model conventions [11]. Simulations are carried out with the Boltzmann factor $\exp(-\beta E)$.

The Wilson action for pure SU(3) non-Abelian Euclidean lattice gauge theory is

$$S_A = \frac{2\cdot 3}{g^2}\sum_{n,\mu\nu}\left[1 - \frac{1}{2\cdot 3}\,\mathrm{Tr}(U_{n,\mu\nu} + \mathrm{H.c.})\right], \tag{2}$$

where $U_{n,\mu\nu} = U_{n,\mu}U_{n+\hat{\mu},\nu}U^{\dagger}_{n+\hat{\nu},\mu}U^{\dagger}_{n,\nu}$ denotes the product of the SU(3) link matrices in the fundamental representation around a plaquette and the sum runs over all plaquettes. Simulations are done with the Boltzmann factor $\exp(S_A)$.

The Markov chain Monte Carlo (MC) process provides model A (Glauber) dynamics in the classification of Ref. [3]. For Potts models we use the heatbath algorithm of [11] and for SU(3) gauge theory the Cabibbo-Marinari [12] heatbath algorithm and its improvements of Ref. [13] (no over-relaxation, to stay in the universality class of Glauber dynamics). In each case a time step is a sweep of systematic updating through the lattice, which touches each degree of freedom once. With small statistics we have checked that updating in random order gives similar results up to a slowing down of the evolution speed by a constant factor. This is expected as in equilibrium simulations random updating has larger autocorrelations than systematic updating [11]. For our equilibrium simulations of Potts models we used a multicanonical [14] Metropolis algorithm.

B. Structure factors

Consider two-point correlation functions defined by

$$\langle u_0(0)u_0^{\dagger}(\vec{j})\rangle_L = \frac{1}{N_\sigma^3}\sum_{\vec{i}} u_0(\vec{i})u_0^{\dagger}(\vec{i}+\vec{j}), \tag{3}$$

where $\vec{i}$ denotes spatial coordinates. Periodic boundary conditions are used and the subscript L on the left-hand side reminds us that the average is taken over the spatial lattice. For gauge systems we deal with fluctuations of the Polyakov loop, for analogue spin systems with fluctuations of the magnetization.

The finite volume continuum limit of (3) is achieved by lattice spacing $a \to 0$ and $N_\sigma \to \infty$ with the physical length of the box $L = aN_\sigma = \text{const}$. This means that

$$\langle u_0(0)u_0^{\dagger}(\vec{j})\rangle_L = \frac{1}{a^3 N_\sigma^3}\sum_{\vec{i}} a^3 u_0(\vec{i})u_0^{\dagger}(\vec{i}+\vec{j}) \tag{4}$$

transforms into

$$\langle u(0)u^{\dagger}(\vec{R})\rangle_L = \frac{1}{L^3}\int d^3 r\, u(\vec{r})u^{\dagger}(\vec{r}+\vec{R}), \tag{5}$$

with $\vec{r} = a\vec{i}$, $\vec{R} = a\vec{j}$, $u(\vec{r}) = u_0(\vec{i})$, and so on. We define the structure function $F(\vec{p})$ as a Fourier transformation of the two-point correlation function (5):

$$F(\vec{p}) = \int \langle u(0)u^{\dagger}(\vec{R})\rangle_L e^{i\vec{p}\,\vec{R}} d^3 R. \tag{6}$$

Periodic boundary conditions imply

$$\vec{p} = \frac{\vec{k}}{a} = \frac{2\pi}{L}\vec{n}, \tag{7}$$

where $\vec{n}$ is an integer vector (0,0,0), (0,0,1), and so on. The discretized version of (6) is

$$F(\vec{p}) = \sum_{\vec{j}} a^3 \langle u_0(0)u_0^{\dagger}(\vec{j})\rangle_L e^{i\vec{k}\,\vec{j}}. \tag{8}$$

Using the definition (3) and shifting the $\vec{j}$ summation, one arrives (after straightforward algebra) at the expression

$$F(\vec{p}) = \frac{a^3}{N_\sigma^3}\left|\sum_{\vec{i}} e^{-i\vec{k}\,\vec{i}} u_0(\vec{i})\right|^2, \tag{9}$$

where we may rewrite the product in the exponent as

$$a\vec{p}\,\vec{i} = \vec{k}\,\vec{i} = \frac{2\pi}{N_\sigma}\vec{n}\,\vec{i}. \tag{10}$$

As we let the system evolve after a quench $u_0(\vec{i})$ becomes time dependent: $u_0(\vec{i}, t)$. The time t corresponds to the dynamical process, i.e., in our case the Markov chain model A dynamics. We consider an ensemble of systems (replica) and dynamical observables are calculated as ensemble averages denoted by $\langle \ldots \rangle$. The time-dependent structure functions averaged over replicas are

$$F_{\vec{p}}(t) = \langle F(\vec{p}, t)\rangle. \tag{11}$$

During our simulations they are averaged over rotationally equivalent momenta and the notation

$$F_i(t) \tag{12}$$

is used for the structure function at momentum

$$\vec{p} = \frac{\vec{k}}{a} = \frac{2\pi}{L}\vec{n} \tag{13}$$

where $|\vec{n}| = n_i$ defines i. The F_i are called structure function modes or structure factors (SFs). We recorded the following modes (including the permutations) n_1: (1,0,0), n_2: (1,1,0), n_3: (1,1,1), n_4: (2,0,0), n_5: (2,1,0), n_6: (2,1,1), n_7: (2,2,0), n_8: (2,2,1) and (3,0,0), n_9: (3,1,0). Note that there is an accidental degeneracy in length for n_8. We also measured higher modes, in some cases up to n_{64}. They exhibit the same behavior as the lower modes, but the data are far more noisy, so that we abstain from reporting these results. A difference from the normalization of [1,2] is that in the present paper we average over the permuted momenta instead of just summing them up. For instance, for the F_1 SF the difference is a multiplicative factor of 3.

III. POTTS MODELS

For the analogue spin models the lattice spacing a cannot be varied. We set $a = 1$, so that the distinction between L and N_σ, $\vec{p}$ and $\vec{k}$ becomes superfluous. We use L and $\vec{k}$ in the following. The normalization of the SFs differs from our previous work [1,2]. It is chosen so that they approach constant values in the infinite volume limit of equilibrium simulations of spin systems at *noncritical* temperatures. This follows from the fact that the random fluctuations in (12) are of order $\sqrt{V} = \sqrt{L^3}$. At a critical temperature of a second order phase transition a divergence of the SFs is then encountered as we illustrate for the 3D Ising model. A sustained increase of a SF with lattice size cannot be stronger than being proportional to $V = L^3$, because an upper bound on each SF is obtained by setting all values in the sum of Eq. (9) equal to 1.

A. Equilibrium results

In this section we compile SF estimates from equilibrium simulations of the 3D Ising and 3-state Potts model on L^3 lattices. Our simulations are carried out in a multicanonical ensemble [14], covering a temperature range from $\beta_{\min} = 0$ (infinite temperature) to $\beta_{\max} > 0$ below the phase transition temperature of the respective system. Instead of relying on a recursion (see, e.g., [11]), the multicanonical parameters were extracted by finite size (FS) extrapolation from smaller to larger systems, which is an efficient way when the FS behavior is controllable.

The advantage of using multicanonical simulations is that accurate values of the SF peaks can be determined from one data set. Reweighting of a canonical simulation [15] allows accurate determination of the maxima of one quantity, but on finite lattices the maxima of different observables are too far apart to be within the reweighting range of one canonical simulation. We find it convenient to have the entire range of interest covered in one simulation. In particular, equilibration of the configurations around the transition and in the ordered phase is then secured due to frequent excursions into the discorded region all the way to $\beta = 0$.

1. 3D Ising model

At the critical point the two-point function on an infinite lattice falls off with a power law, which defines the critical exponent η:

$$f(\vec{x}) = \langle s(\vec{0})s(\vec{x})\rangle \sim |\vec{x}|^{-d+2-\eta}, \qquad |\vec{x}| \to \infty. \tag{14}$$

This determines the low-momentum behavior of the Fourier transformation $F(\vec{k})$. Namely,

$$\begin{aligned}\hat{F}(\lambda\vec{k}) &\sim \int d^d x e^{i\lambda\vec{k}\cdot\vec{x}}|\vec{x}|^{-d+2-\eta} \\ &= \int \frac{d^d x'}{\lambda^d} e^{i\vec{k}\cdot\vec{x}'}\lambda^{d-2+\eta}|\vec{x}'|^{-d+2-\eta} \\ &\sim \lambda^{\eta-2}\hat{F}(\vec{k})\end{aligned}$$

holds and, therefore,

$$\hat{F}(\vec{k}) \sim |\vec{k}|^{-b}, \qquad b = 2 - \eta, \quad \text{for } |\vec{k}| \to 0. \tag{15}$$

For fixed $\vec{n}$ we have $\vec{k} = 2\pi\vec{n}/L$ and we find for any fixed value of $\vec{n}$ the finite size scaling (FSS) divergence

$$\hat{F}_{\vec{n}} \sim L^b, \qquad b = 2 - \eta, \quad \text{for } L \to \infty \tag{16}$$

with lattice size.

The infinite volume phase transition temperature of the 3D Ising model is estimated to be $\beta_c = 0.221\,57(3)$; e.g., see [16]. In our multicanonical simulations we cover the range from $\beta_{\min} = 0$ to $\beta_{\max} = 0.25$, well including the transition region. Table I gives an overview of the lattice sizes and the accumulated statistics (a sweep updates each spin once) together with our estimate of the maximum values $F_1^{\max}$ of the first SF, evaluated at the value β_m.

TABLE I. Statistics and SF maxima $F_1^{\max}$ at β_m from our equilibrium simulations of the 3D Ising model on L^3 lattices.

L	Sweeps	$F_1^{\max}$	β_m	Cycles
20	$32 \times 5 \cdot 10^4$	17.00 (26)	0.219 874	83
30	$32 \times 2 \cdot 10^5$	37.97 (70)	0.220 825	89
44	$32 \times 6 \cdot 10^5$	78.4 (1.6)	0.221 146	70
56	$32 \times 1 \cdot 10^6$	129.6 (2.7)	0.221 345	45
66	$32 \times 1.6 \cdot 10^6$	175.6 (4.9)	0.221 387	43
80	$64 \times 2 \cdot 10^6 \times 3$	257.4 (2.4)	0.221 462	65 + 72 + 67

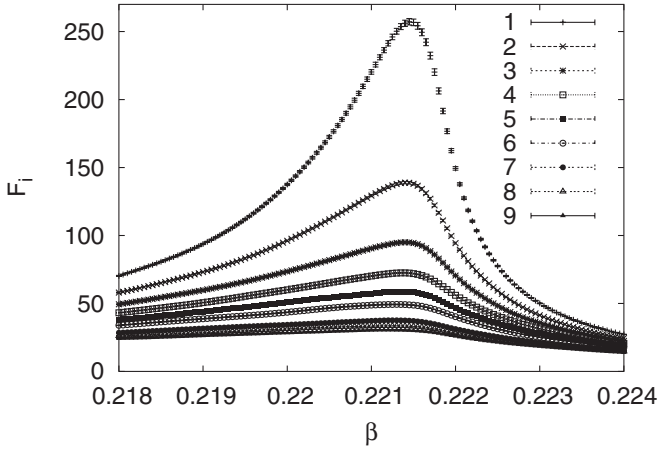

FIG. 1. SFs $F_i, i = 1, \ldots, 9$ from simulations of the Ising model on an 80^3 lattice.

Error bars are given in parentheses and apply to the last digits of the number in front. They are calculated with respect to a number of jackknife bins given by the first number in column 2 of the table, and the multicanonical reweighting procedure uses the logarithmic coding described in [17]. Three independent runs were carried out for the $L = 80$ lattice. Before starting with measurements we normally performed the number of sweeps of one measurement bin for reaching equilibrium. This is sufficient because equilibration problems are mild in multicanonical simulations. Running time for each of our $L = 80$ simulations was about three months on a 2 GHz Athlon PC. The last column of Table I gives the number of cycles,

$$(\beta_e \leq \beta_{\min}) \rightarrow (\beta_e \geq \beta_{\max}) \rightarrow (\beta_e \leq \beta_{\min}),$$

which the Markov process performed during the production run, where β_e is the effective energy-dependent β of the multicanonical procedure.

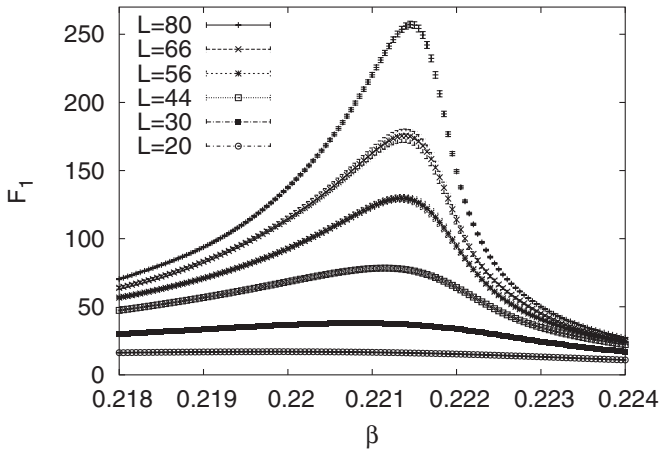

FIG. 2. Finite size behavior of SF F_1 from Ising model simulations on L^3 lattices.

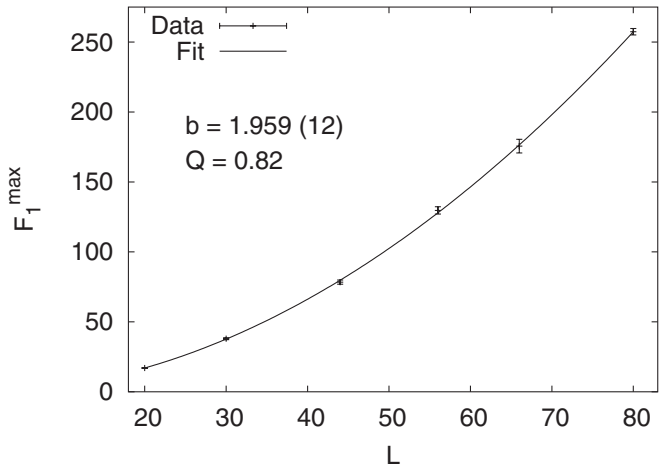

FIG. 3. Fit of the $F_1^{\max}$ maxima of Table I to the FSS form (16).

For our largest lattice, the SFs 1–9 are plotted in Fig. 1, where we restrict β to a neighborhood of the critical temperature. Each SF develops a clear peak, only that the peaks for the higher SFs are less pronounced than those for the lower. In particular, the scale of the figure does not resolve the peaks for the SFs ≥ 7 anymore. These peaks are found on a reduced scale and for each SF the FSS behavior (16) holds. However, the numerical accuracy decreases with increasing $|\vec{k}|$. So we are content with simply analyzing the FSS behavior of SF 1. Figure 2 shows SF 1 for all our lattice sizes and the maxima values are collected in Table I. A two parameter fit to the form (16) is shown in Fig. 3. It gives $b = 1.959\,(12)$ with a goodness of fit $Q = 0.82$ (for the definition of Q see, e.g., Ref. [11]), a result well compatible with the high precision estimates $\eta = 0.0364\,(5)$ given in the review article [18] on critical phenomena and renormalization group theory.

2. 3D 3-state Potts model

For the 3D 3-state Potts model one deals with a relatively weak first order phase transition at $\beta_c = 0.275\,272\,0\,(49)$, a value which averages two somewhat inconsistent ($Q = 0.003$ for the Gaussian difference test) estimates of the literature [19] (because of the inconsistency the error bars are averaged here and not reduced). In our multicanonical simulations we cover the range from $\beta_{\min} = 0$ to $\beta_{\max} = 0.33$. An overview of the statistics and

TABLE II. Statistics and SF maxima $F_1^{\max}$ at β_m for our equilibrium simulations of the 3D 3-state Potts model on L^3 lattices.

L	Sweeps	$F_1^{\max}$	β_m	Cycles
20	$32 \times 1.2 \cdot 10^5$	19.00 (22)	0.274 273	59
30	$32 \times 5.2 \cdot 10^5$	38.11 (41)	0.274 924	71
40	$32 \times 1.5 \cdot 10^6$	60.30 (50)	0.275 116	73
50	$126 \times 1.5 \cdot 10^6$	80.46 (55)	0.275 181	131

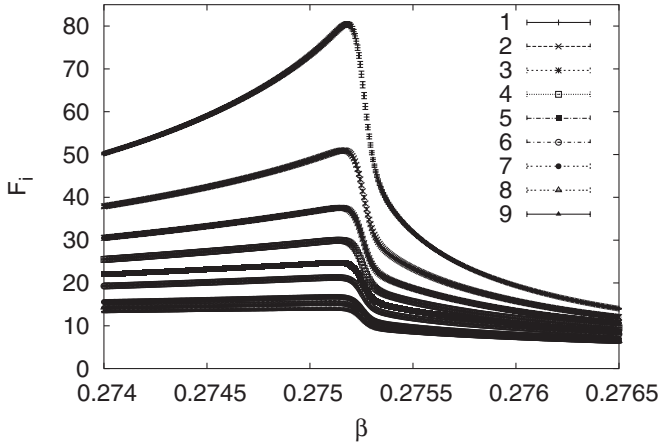

FIG. 4. SFs $F_i, i = 1, \ldots, 9$ from simulations of the 3-state Potts model on a 50^3 lattice.

some results are given in Table II, similarly as before for the 3D Ising model in Table I.

For our 50^3 lattice the SFs 1–9 are plotted in Fig. 4, where we restrict β to a neighborhood of the transition temperature. As for the 3D Ising model each SF develops a clear peak, but the shapes are significantly different. A relatively smooth increase is followed by a rather abrupt decrease. The lattice size dependence of SF 1 is depicted in Fig. 5, which indicates (as expected) that the abrupt decrease develops into a discontinuity for $L \to \infty$. The increase of the structure function maxima is irregular and smaller from $L = 40$ to $L = 50$ than from $L = 30$ to $L = 40$. Asymptotically, for $L \to \infty$ a finite maximum value is expected in the case of a first order phase transition. Within our limited lattice sizes this is not yet seen, but a power law fit (16) of the type used in Fig. 3, which is the large L behavior in the case of a second order transition, becomes entirely inconsistent: $Q = 2.7 \times 10^{-11}$ is the goodness of fit obtained.

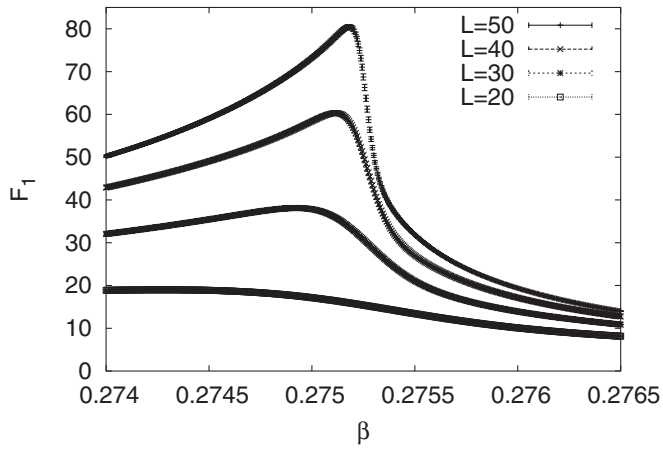

FIG. 5. Finite size behavior of SF F_1 from 3-state Potts model simulations on L^3 lattices.

TABLE III. Repetitions of quenches from $\beta = 0.2$ to β_f for the 3D 3-state Potts model on L^3 lattices.

$\beta_f \backslash L$	20	40	60	80	100	120
0.3	640	640	640	320	320	320
0.27	640	320	320	32		

B. Quenches

After outlining the equilibrium scenario, let us discuss the time evolution after a quench from the disordered into the ordered phase of the 3D 3-state Potts model. An overview of our statistics is given in Table III. We quench from $\beta = 0.2$ to the β_f value given in the table, which collects the numbers of repetitions of each quench. Error bars are then calculated with respect to 32 bins. Larger lattices exhibit self-averaging, so that one needs less repetitions than for smaller lattices.

In previous work [2] we have investigated the quench $\beta = 0.2 \to 0.3$ and its subsequent stochastic time evolution on lattices up to size 80^3. Meanwhile we have extended the SF part of this investigation to lattices of size up to 120^3 and Fig. 6 shows the time evolution of SF 1 after this quench. Note that we divide the SF by an extra volume factor in this figure. So its initial increase with lattice size is faster than $\sim V$, the maximum sustained increase we discussed in the first paragraph of Sec. III. For our largest lattices, $L \geq 80$, the increase appears to level off to precisely

$$F_1^{\max}(L) \sim V = L^3 \quad \text{for } L \to \infty. \tag{17}$$

Heuristically this behavior during spinodal decomposition may be expected: The quench changes the temperature in the entire lattice instantaneously. It is then plausible that the local contribution to the SF is, on the average, everywhere the same. So one expects an increase $\sim V$ of the maxima. The initial overshooting may be explained by an

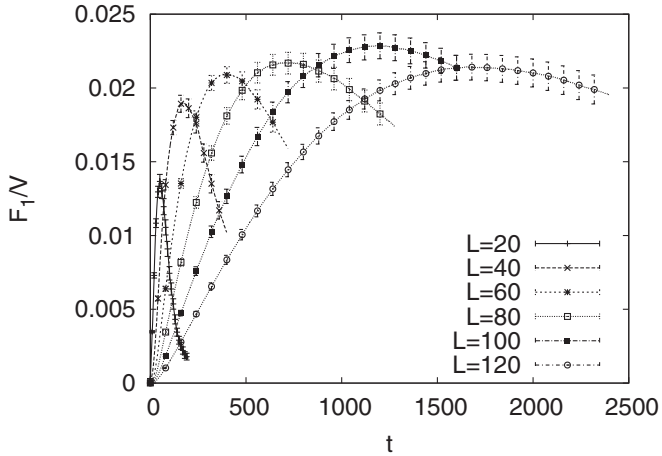

FIG. 6. Time evolution of SF F_1 for the 3-state Potts model on L^3 lattices after a quench from $\beta = 0.2 \to 0.3$.

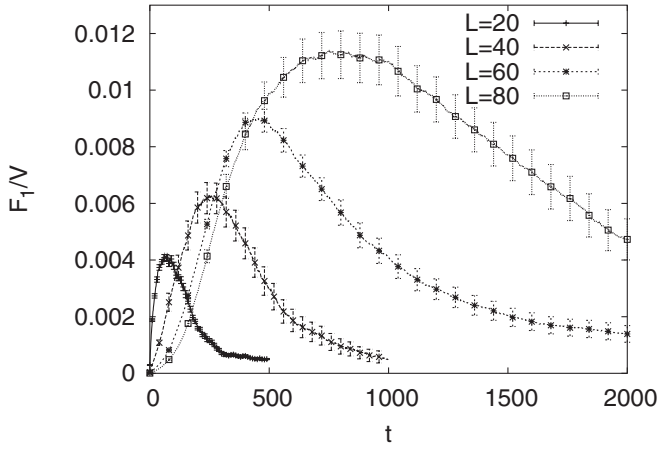

FIG. 7. Time evolution of SF F_1 for the 3-state Potts model on L^3 lattices after a quench from $\beta = 0.2 \rightarrow 0.28$.

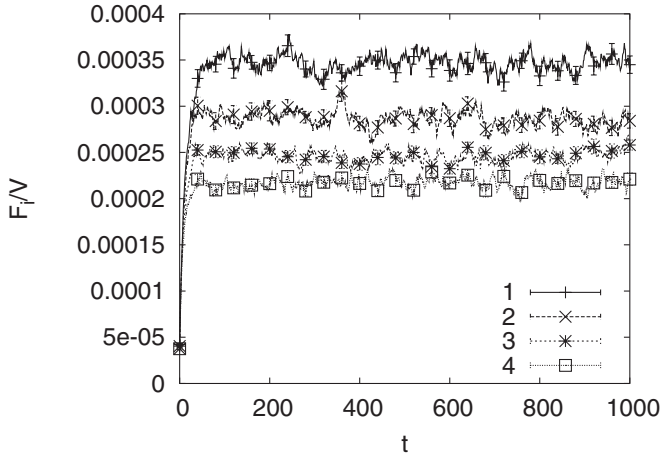

FIG. 9. Time evolution of SFs F_i, $i = 1, \ldots, 4$ for the 3-state Potts model on a 40^3 lattice after a quench below β_c from $\beta = 0.2 \rightarrow 0.27$.

increase of correlations with lattice size, which levels off once the lattice size exceeds the correlation length.

To test how this growth of the signal proportional to the volume depends on the depth of the quench into the ordered region, we performed a quench to a temperature closer to the transition temperature, $\beta = 0.2 \rightarrow 0.28$. As shown in Fig. 7 we find the same phenomenon as before: The maximum sustained increase $\sim V$ is initially overshot. The growth of the signal is weaker than before, as is expected since the system does not change so drastically.

In both figures we see that the time positions $t^{\max}$ of the SF 1 maxima move towards larger values with increasing lattice size. For our two quenches $t^{\max}(L)$ is plotted in Fig. 8 on a log-log scale. With parameters a_0 and a_1 both curves can consistently be fitted to the expected form

$$t^{\max}(L) = a_0 + a_1 L^2. \tag{18}$$

As t is measured in units of sweeps, the number of spin updates per time unit does not depend on L. In spin systems, t is thus proportional to the physical time. After

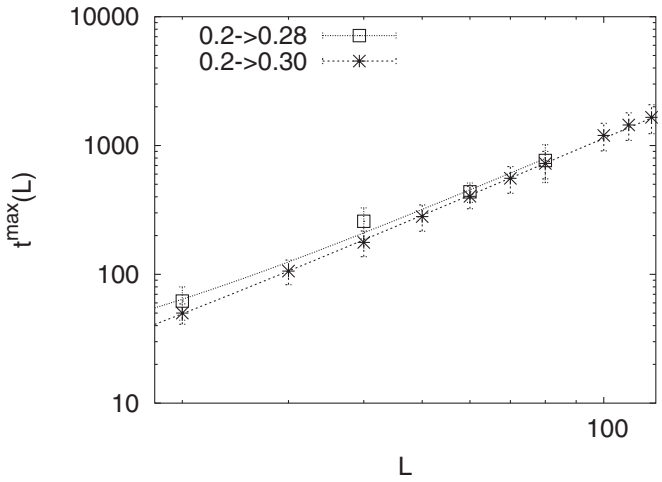

FIG. 8. Time positions of the SF F_1 maxima versus lattice size.

the quench into the ordered phase the infinite spin system cannot be equilibrated in any finite time, a fact known in condensed matter physics [20]. The explanation for this phenomenon is that the system grows initially competing domains of three distinct orientations. To dissolve these domains by local random fluctuations until one of them dominates the entire lattice is a slow process, which requires of order L^2 time.

Visualization of these domains faces difficulties, because naive geometrical definitions do not work. Compare Fig. 8 of Ref. [2]. For analogue Potts models this is overcome by the Fortuin-Kasteleyn [21] cluster definition, but there is no immediate generalization to gauge theories, although promising ideas have been published [22]. Here we do not investigate this question any further. We think that it is safe to assume that competing domains are, in both spin and gauge systems, the underlying cause for the explosive growth of structure factors $F_i(t)$, which we encounter in their time evolution after a heating quench.

Finally, in this section, based on 640 repetitions, Fig. 9 demonstrates that for a quench below the critical β nothing more than a smooth transition from one equilibrium value to the next happens. Therefore the explosive growth of SFs is an unambiguous signal that β_f is indeed in the ordered phase.

IV. SU(3)

We report results from quenches of pure SU(3) lattice gauge theory on $N_\tau N_\sigma^3$ lattices. Our statistics is summarized in Tables IV and V. All quenches are from the initial value $6/g^2 = 5.5$. The $4 \times N_\sigma^3$ simulations of Table IV were already reported in [10]. The simulations for the other lattices are new. The difference between the tables is that for the lattices of Table IV we follow the quench all the way to its equilibrium value at T_f, while for the lattices of Table V we calculated only the initial increase of the SFs as

TABLE IV. Quenches from $6/g^2 = 5.5$ to $6/g_f^2$ for pure SU(3) lattice gauge theory (n denotes the number of repetitions).

Lattice	T_f/T_c	$6/g_f^2$	n	T_f/T_c	$6/g_f^2$	n
4×16^3	1.250	5.802 740	10 000	1.568	5.920 000	10 000
4×32^3	...	...	...	1.568	5.920 000	4000
4×64^3	...	...	...	1.568	5.920 000	170
6×24^3	1.250	6.022 334	6000	1.568	6.165 427	6000
8×32^3	1.250	6.206 036	3000	1.568	6.364 572	3000

TABLE V. Initial quenches from $6/g^2 = 5.5$ to $6/g_f^2$ for pure SU(3) lattice gauge theory (n as in Table IV).

Lattice	T_f/T_c	$6/g_f^2$	n	T_f/T_c	$6/g_f^2$	n
4×32^3	1.250	5.802 740	3000	...	...	...
4×64^3	1.250	5.802 740	140	...	...	...
6×48^3	1.250	6.022 334	600	1.568	6.165 427	750
6×60^3	1.250	6.022 334	200	1.568	6.165 427	200
8×56^3	1.250	6.206 036	1000	1.568	6.364 572	1000

needed for the determinations of critical modes in Sec. IV B.

The new data serve to study the quantum continuum limit $a \to 0$ (in physical units like fermi). The final values g_f^2 of the bare coupling constants are chosen, so that the values of T_f/T_c stay at the fixed ratios given in the table. For this we take (substantial) corrections to the two-loop equation of Lambda lattice into account, which follow from renormalization group results tabulated in Ref. [23]. As the use of tables is tedious, we like to mention that, with an accuracy of 0.5% and better, our T_f/T_c values are reproduced by using the formula

$$\Lambda_L(g^2) = \Lambda_L^{as}(g^2)\lambda(g^2) \tag{19}$$

where $\Lambda_L^{as}(g^2)$ is given by (e.g., [24])

$$a\Lambda_L^{as} = (b_0 g_0^2)^{-b_1/(2b_0^2)} e^{-1/(2b_0 g^2)}$$

with $b_0 = \frac{11}{3}\frac{N_c}{16\pi^2}$, $b_1 = \frac{34}{3}(\frac{N_c}{16\pi^2})^2$ and

$$\lambda(g^2) = 1 + a_1 e^{-a_2/g^2} + a_3 g^2 + a_4 g^4$$

with $a_1 = 715\,537\,50$, $a_2 = 19.480\,99$, $a_3 = -0.037\,724\,73$, and $a_4 = 0.508\,905\,2$.

For $N_\tau = 4$, fixed, Fig. 10 shows the divergence of the SF 1 maxima with increasing lattice size N_σ^3 as well as a $t^{\max}(N_\sigma) \sim N_\sigma^2$ behavior in complete analogy to our results for Potts models. All the lattices of Fig. 10 are quenched to the bare coupling constant $g_f^2 = 6/5.92$. Therefore the time scale of the Markov process (determined by the Boltzmann factors) is the same on all these lattices and up to an unknown multiplicative factor identified with that of a dissipative, nonrelativistic dynamics. Nonrelativistic does not necessarily mean that the propagation of the signal through the lattice is slow. On the contrary, Galilee transformations set no upper limit on speeds. Our quench changes the temperature instantaneously through the entire lattice, while the subsequent propagation of the response proceeds through local interactions.

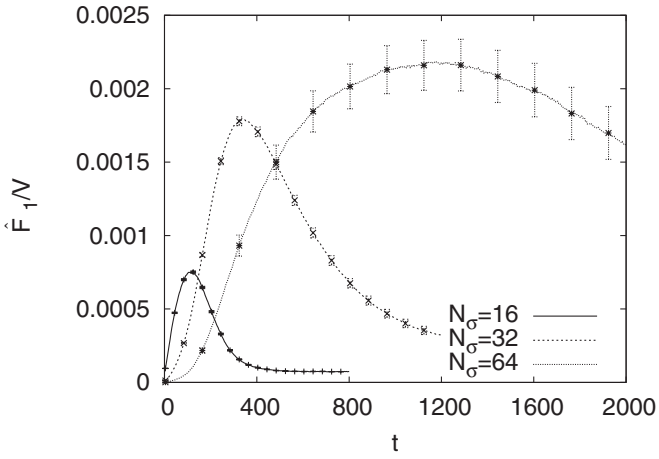

FIG. 10. Time evolution of SF F_1/V for SU(3) lattice gauge theory on $4 \times N_\sigma^3$ lattices after a quench $6/g^2 = 5.5 \to 5.92$.

A. Finite volume continuum limit

In the following we illustrate the approach of the limit $a \to 0$, $L = \text{const}$, $T_f/T_c = \text{const}$, by increasing N_τ from 4 to 6 to 8 and the volume N_σ^3 from $N_\sigma = 16$ to 24 to 32, so that the ratio N_σ/N_τ stays constant. The ratio of temperatures T_f/T_c is kept constant by using Eq. (19) to determine the appropriate bare coupling constant values for each N_τ. Because of the divergence of (bare) Polyakov loop correlations we face a renormalization problem, which we overcome by dividing all SFs F_i by their equilibrium values at T_f, $F_{i,f}$. The time-scale situation changes too, because we have to use different bare coupling constant values for different N_τ. As one knows that a finite physical volume equilibrates in a finite time, we fix this normalization problem by rescaling the time axis to

$$t' = \frac{t}{\lambda_t(N_\tau, T_f/T_c)} \tag{20}$$

so that all maxima fall on top of one another. We do not lose information as we anyhow do not know the overall normalization factor for our time scale.

Figures 11 and 12 show the time evolution of the $F_1/F_{1,f}$ SFs for our two T_f/T_c values. The time axis of our original measurements in units of sweeps are related to those used in Fig. 11 by the $\lambda_t(N_\tau, 1.25)$ factors 1:2.655:5.457 for the N_τ values 4:6:8, respectively. For Fig. 12 the corresponding $\lambda_t(N_\tau, 1.568)$ ratios are 1:2.768:6.362. The maxima of the curves decrease when increasing N_τ from 4 to 6 to 8. As the decrease slows down with increasing lattice size, there is some evidence for an approach to a shape, which represents the continuum limit.

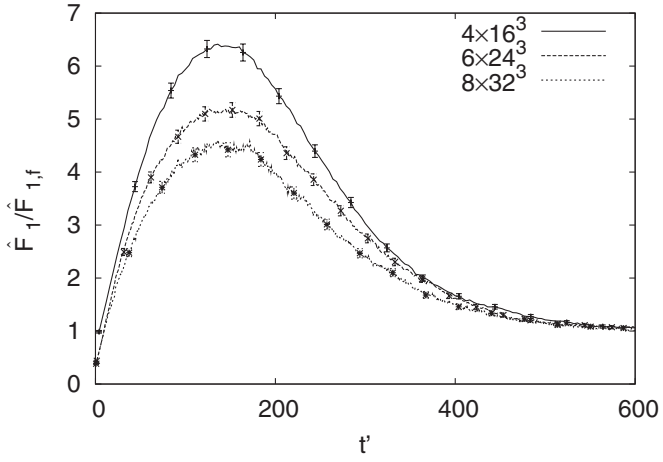

FIG. 11. Time evolution of SF $F_1/F_{1,f}$ for SU(3) lattice gauge theory on $N_\tau N_\sigma^3$ lattices of constant physical volume of a quench to $T_f/T_c = 1.25$.

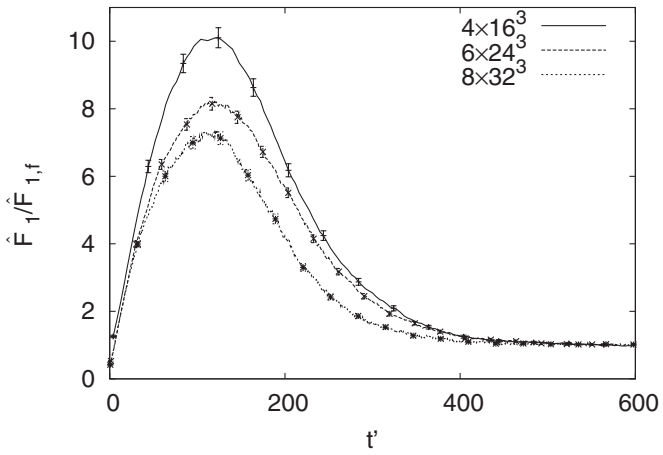

FIG. 12. Time evolution of SF $F_1/F_{1,f}$ for SU(3) lattice gauge theory on $N_\tau N_\sigma^3$ lattices of constant physical volume of a quench to $T_f/T_c = 1.568$.

B. Debye screening mass

The current understanding of the early time evolution of systems out of equilibrium is largely based on investigating stochastic equations which are dynamical (time-dependent) generalizations of the Landau-Ginzburg effective action models of the static (equilibrium) theory [3,25]. For model A the linear approximation results in the following equation for a SF:

$$\frac{\partial \hat{F}(\vec{p}, t)}{\partial t} = 2\omega(\vec{p})\hat{F}(\vec{p}, t), \tag{21}$$

with the solution

$$\hat{F}(\vec{p}, t) = \hat{F}(\vec{p}, t = 0)\exp(2\omega(\vec{p})t), \quad \omega(\vec{p}) > 0 \quad \text{for } |\vec{p}| > p_c, \tag{22}$$

where $p_c > 0$ is a critical momentum. Originally the linear theory was developed for model B [26,27]. Details for model A can be found in Refs. [2,28].

From our measurements of $F(\vec{p}, t)$ on the $N_\tau = 4$, 6 and 8 lattices, we find straight line fits to the form $\omega(p) = a_0 + a_1 p^2$, $p = |\vec{p}|$ with a negative slope a_1. They determine the critical momentum p_c as the value where $\omega(p)$ changes its sign. The fits for $T_f/T_c = 1.25$ are shown in Fig. 13 and for $T_f/T_c = 1.568$ in Fig. 14, where we introduced

$$\omega'(p) = \lambda_t(N_\tau, T_f/T_c)\omega(p). \tag{23}$$

This definition absorbs the shift (20) of the time scale, so that $\omega'(p)t' = \omega(p)t$ holds. It is only in the primed variables that one realizes an eventual approach to the continuum limit from Figs. 13 and 14. In particular, note that for $T_f/T_c = 1.568$ the $N_\tau = 6$ and 8 fits are identical within statistical errors. The obtained values for $p_c(N_\tau)/T_c$ are listed in Table VI. The (finite volume) continuum limit is extrapolated by fitting these values to the form

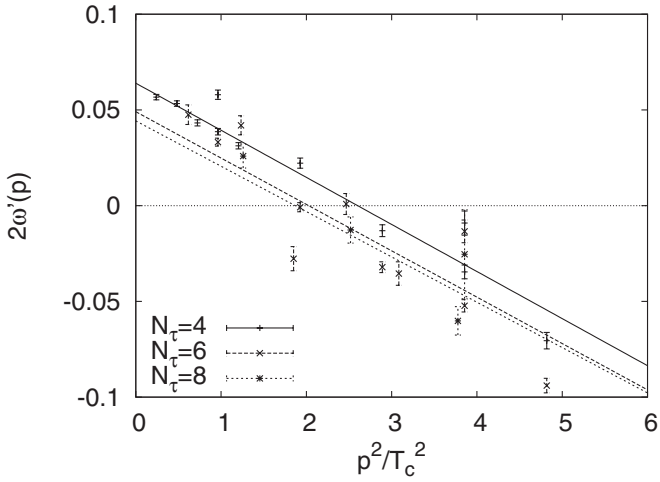

FIG. 13. SU(3) determination of p_c for $T_f/T_c = 1.25$.

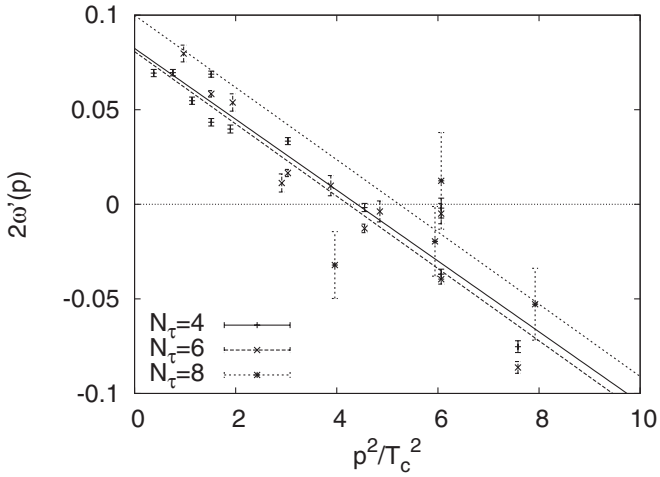

FIG. 14. SU(3) determination of p_c for $T_f/T_c = 1.568$.

TABLE VI. Fit results for p_c/T_c.

Lattice size:	$N_\tau = 4$	$N_\tau = 6$	$N_\tau = 8$	∞
$T_f/T_c = 1.25$:	1.613 (18)	1.424 (26)	1.37 (10)	1.058 (79)
$T_f/T_c = 1.568$:	2.098 (19)	2.058 (22)	2.29 (15)	2.006 (73)

$$\frac{p_c(N_\tau)}{T_c} = \frac{p_c}{T_c} + \frac{\text{const}}{N_\tau} \tag{24}$$

with the results given in the last column of Table VI.

Relying on a phenomenological analysis by Miller and Ogilvie [9], p_c is related by

$$m_D = \sqrt{3} p_c \tag{25}$$

to the Debye screening mass at the final temperature T_f after the quench. We get

$$m_D = 1.83(14) T_c \quad \text{for } T_f/T_c = 1.25, \tag{26}$$

$$m_D = 3.47(13) T_c \quad \text{for } T_f/T_c = 1.568. \tag{27}$$

The value at $T_f/T_c = 1.568$ is in excellent agreement with a determination of $m_D(T)$ from a best-fit analysis of the large distance part of the color singlet free energies [29]. This supports that the simulated dynamics bears physical content. Our estimate at $T_f/T_c = 1.25$ is by a factor of 2 smaller than the one of Ref. [29]. This is not really a surprise, because $T_f/T_c = 1.25$ is close to the spinodal end point, so that the derivation [9] of the relationship (25) is no longer valid.

For pure SU(3) lattice gauge theory $T_c = 265(1)$ MeV holds, assuming $\sigma = 420$ MeV for the string tension, while for QCD the crossover temperature appears to be around $T_c \approx 165$ MeV; see Ref. [30] for reviews. Using for simplicity $T_c = 200$ MeV to illustrate the magnitudes, the temporal lattice size is then about 1 F at T_c. The spatial sizes of our lattices used in this section reach up to (8 fermi)^3. At the T_f values the edge lengths are shortened by the corresponding T_c/T_f factors; i.e., the volume is (6.4 fermi)^3 for $T_f/T_c = 1.25$ and (5.10 fermi)^3 for $T_f/T_c = 1.568$. The screening length associated with the Debye mass, $\xi_D = 1/m_D$, is then approximately 0.6 F at $T_f/T_c = 1.25$ and 0.3 F at $T_f/T_c = 1.568$. The illustration of the finite volume continuum limit in Sec. IVA was for lattices of size (4 fermi)^3 at T_c, i.e., (3.2 fermi)^3 at $T_f/T_c = 1.25$ and (2.55 fermi)^3 at $T_f/T_c = 1.568$. Our volumes are smaller than the envisioned deconfined region of about (10 fermi)^3 in relativistic heavy-ion experiments. Because of periodic boundary conditions one may expect that MC simulations on smaller lattices are representative for the central region of the larger volume. Our result is that the Debye screening length is short on the scale of the deconfined region.

C. Measurements near structure factor maxima versus deconfined equilibrium

For SU(3) gauge theory the triality of Polyakov loops with respect to the Z_3 center of the gauge group takes the place of the spin orientations in the 3D 3-state Potts model. Although a satisfactory cluster definition does not exist for gauge theories, the underlying mechanism of competing vacuum domains is expected to be similar to the one in the spin models. To study their influence on Polyakov loop correlations and on the gluonic energy ϵ and pressure p densities, we calculate these quantities at times $t \le t_{\max}$ as well as at $t > t_{\max}$.

Our structure function measurements gave "on the fly" two-point correlations between Polyakov loops defined by

$$C_o(d, t) = \langle P(0, t) P(d, t) \rangle_L - (\langle |P(0, t)| \rangle_L)^2 \tag{28}$$

where the averaging procedures are those we discussed after Eq. (3) and $d = 1, 2, \sqrt{2}, \ldots$. The value of these results is somewhat limited, because our focus was not on good equilibrium results and the stored data do not allow us to project onto particular channels of the free energy of static quarks (which lead to larger correlation lengths than those obtained). For several values of d we plot in Fig. 15 the time development of $C_o(d)$ on our largest lattice using the t' time scale (20). The correlations assume maxima at about the same time values $t_{\max}$ for which the SFs peak, although less pronounced. In Fig. 16 we plot the d dependence for the time values $0.5t_{\max}$, $t_{\max}$, and $5t_{\max}$. At $5t_{\max}$ fits of the form $C_o(d) \sim \exp(-m_P a d)/(ad)$, where a is the lattice spacing, give the m_P estimates which are collected in Table VII. The last column of this table gives infinite volume estimates obtained from fits of the form (24). In contrast to that, large correlations are found at $0.5t_{\max}$ and $t_{\max}$, which are fully consistent with a power law.

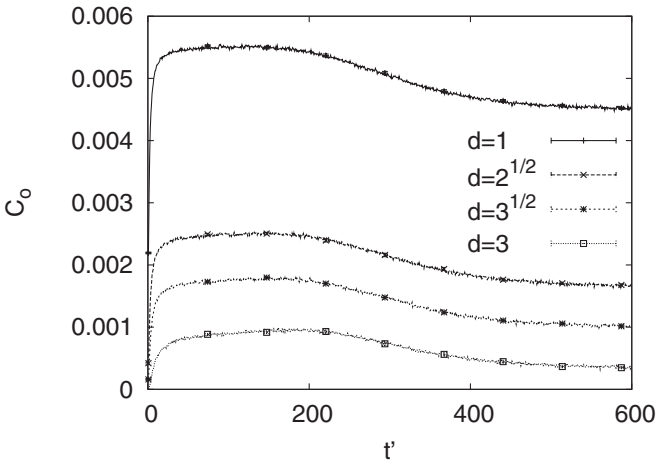

FIG. 15. Time dependence of Polyakov loop correlations $C_o(d)$ on the 8×32^3 lattice for $T_f/T_c = 1.25$ and various d values.

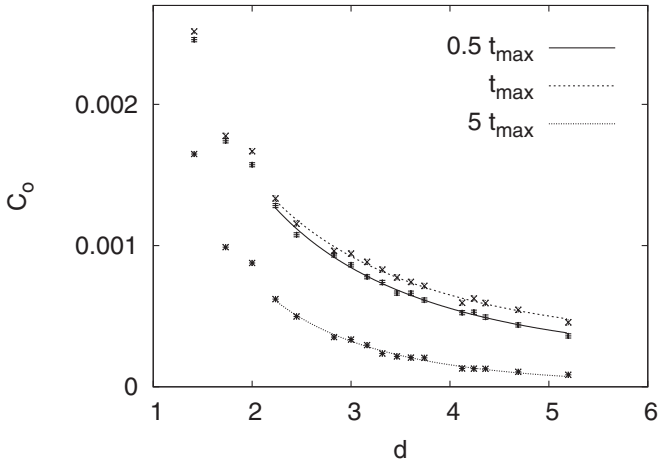

FIG. 16. Falloff behavior of the Polyakov loop correlations of Fig. 15 at different times.

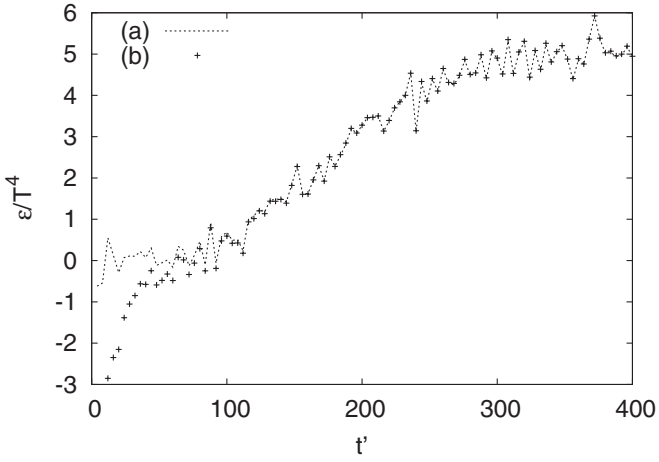

FIG. 17. SU(3) gluonic energy density on the 4×16^3 lattice: (a) with P_0 calculated from the time series after the quench and (b) using equilibrium values for P_0.

The equilibrium procedure for calculating the gluonic energy ϵ and pressure p densities is summarized in Refs. [23,31] (in earlier work [32] the pressure exhibited a nonphysical behavior after the deconfining transition and the energy density approached the ideal gas limit too quickly because the anisotropy coefficients were calculated perturbatively). We denote expectation values of spacelike plaquettes by P_σ and those involving one time link by P_τ. The energy density and pressure can then be cast into the form

$$\frac{\epsilon + p}{T^4} = \frac{8N_c N_\tau^4}{g^2}\left[1 - \frac{g^2}{2}[c_\sigma(a) - c_\tau(a)]\right](P_\sigma - P_\tau) \tag{29}$$

and

$$\frac{\epsilon - 3p}{T^4} = 12N_c N_\tau^4[c_\sigma(a) - c_\tau(a)][2P_0 - (P_\sigma + P_\tau)], \tag{30}$$

where P_0 is the plaquette expectation value on a symmetric ($T = 0$) lattice, and the *anisotropy coefficients* $c_{\sigma,\tau}(a)$ are defined by

$$c_{\sigma,\tau}(a) \equiv \left(\frac{\partial g_{\sigma,\tau}^{-2}}{\partial \xi}\right)_{\xi=1}. \tag{31}$$

They are related to the QCD β function and can be calculated using Padé fits of [23]. To normalize to zero temperature, plaquette values from the symmetric $N_\tau =$ N_σ lattice are needed in Eq. (30). As one stays on the symmetric lattice within the confined phase its equilibration after the quench is fast. Therefore it is enough to use equilibrium values of P_0 at β_f after the quench. This is illustrated in Fig. 17.

In Fig. 18 we show the time evolution of the gluonic energy densities (upper curves) and pressure densities (lower curves) for the $T_f/T_c = 1.25$ quench on our 4×16^3, 6×24^3, and 8×32^3 lattices using the rescaled time definition (20). The curves for the last two lattices fall almost on top of one another, indicating their neighborhood to the continuum limit. The approach to the final equilibrium values is rather smooth. Gluonic energy density mean values at $t_{\max}$ are less than $1/4$ of their final values, while the pressure density is at about $1/3$. In contrast to the shift in the mean value, the widths of the distributions are almost the same at $t_{\max}$ and in the decon-

TABLE VII. Fit results for m_P/T_c at $5t_{\max}$.

Lattice size:	4×16^3	6×24^3	8×32^3	∞
$T_f/T_c = 1.25$:	3.27 (19)	3.70 (20)	4.43 (27)	5.23 (49)
$T_f/T_c = 1.568$:	4.82 (61)	5.33 (35)	6346 (38)	7.70 (95)

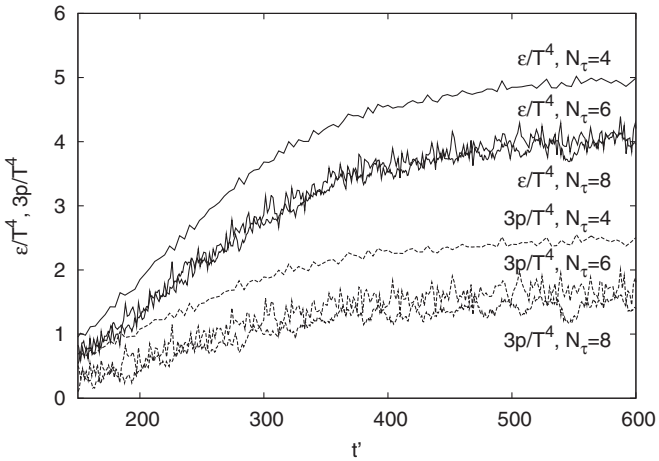

FIG. 18. SU(3) gluonic energy densities and pressures at $T_f/T_c = 1.25$.

fined equilibrium. Results for the $T_f/T_c = 1.568$ quench are quite similar.

V. SUMMARY AND CONCLUSIONS

In equilibrium at temperatures much higher than the deconfinement temperature T_c the perturbative prescription of QCD is that of a weakly coupled gas of quasiparticles. In contrast, recent experiments at the BNL relativistic heavy-ion collider (RHIC) show coherence in particle production and strong collective phenomena, which are well described by the model of a near-perfect, strongly coupled fluid [33]. Nonperturbative effects are expected to play some role in the prescription of equilibrium QCD at temperatures reached at RHIC. For the $T_f/T_c = 1.25$ and $T_f/T_c = 1.568$ temperatures investigated in this paper equilibrium lattice calculations indeed indicate corrections (compare Fig. 7 of [23]). However correlations are typically over ranges much smaller than the size of the deconfined plasma; compare our estimates of the Debye screening mass $m_D(T_f)$. The agreement of our m_D value at $T_f/T_c = 1.568$ with direct equilibrium estimates [29] gives us confidence that model A dynamics reflects physical features.

If the phenomenological description of a strongly coupled plasma implies correlations over distances exceeding 1 F, the time evolution of our structure factors (SFs) depicted in Figs. 6–8 and 10 suggests a scenario in which the deconfined equilibrium phase has actually not been reached at RHIC, but the heating process gets stuck during the time period of explosive growth of the SFs. While this explains correlation over distances much larger than 1 F, it also provides an *unambiguous signal* for the existence of the deconfining phase: Fig. 9 demonstrates that the explosive growth is absent for a quench to a final temperature below T_c.

In real QCD there are two effects which prevent the divergence of the equilibration time shown in Fig. 8: (1) Quarks break the Z_3 symmetry of the SU(3) gauge group, similarly as a magnetic field breaks the degeneracy of the spins in the 3D 3-state Potts model. The final magnitude of the equilibration time depends then on the strength of the breaking as illustrated in Ref. [2] for a weak magnetic field. (2) At RHIC the physical volume is finite, so that even in the case of an exact symmetry the equilibration time is finite. So the scenario in which the system gets stuck during the spinodal decomposition of its vacuum structure could only be based on phenomenological observations. Questions like how a perfect fluid may look during the period of spinodal decomposition arise. Minkowski space simulations of hyperbolic differential equations, which emerge from effective actions for Polyakov loops [34,35], may shed light on the question of whether features observed in the paper are special to Glauber dynamics or are of some universal nature.

ACKNOWLEDGMENTS

This work was in part supported by the DOE Grant No. DE-FG02-97ER41022 at FSU and No. NSF-PHY-0309362 at UCLA. The simulations were performed on PC clusters at FSU and UCLA.

[1] B. A. Berg, U. M. Heller, H. Meyer-Ortmanns, and A. Velytsky, Phys. Rev. D **69**, 034501 (2004).
[2] B. A. Berg, H. Meyer-Ortmanns, and A. Velytsky, Phys. Rev. D **70**, 054505 (2004).
[3] P. M. Chaikin and T. C. Lubensky, *Principles of Condensed Matter Physics* (Cambridge University Press, Cambridge, 1997), p. 467, Table 8.6.1.
[4] R. J. Glauber, J. Math. Phys. (N.Y.) **4**, 294 (1963).
[5] B. Svetitsky and L. G. Yaffe, Nucl. Phys. **B210**, 423 (1982).
[6] R. J. Baxter, J. Phys. C **6**, L445 (1973); F. Y. Wu, Rev. Mod. Phys. **54**, 235 (1982); C. Borgs and W. Janke, J. Phys. I (France) **2**, 2011 (1992).
[7] J. Berges and I.-O. Stamatescu, Phys. Rev. Lett. **95**, 202003 (2005).
[8] E. T. Tomboulis and A. Velytsky, Phys. Rev. D **72**, 074509 (2005).
[9] T. R. Miller and M. C. Ogilvie, Nucl. Phys. B, Proc. Suppl. **106**, 537 (2002); Phys. Lett. B **488**, 313 (2000).
[10] A. Bazavov, B. A. Berg, and A. Velytsky, Int. J. Mod. Phys. A **20**, 3459 (2005).
[11] B. A. Berg, *Markov Chain Monte Carlo Simulations and Their Statistical Analysis* (World Scientific, Singapore, 2004).
[12] N. Cabibbo and E. Marinari, Phys. Lett. B **119**, 387 (1982).
[13] K. Fabricius and O. Hahn, Phys. Lett. B **143**, 459 (1984); A. D. Kennedy and B. J. Pendleton, Phys. Lett. B **156**, 393 (1985).
[14] B. A. Berg and T. Neuhaus, Phys. Rev. Lett. **68**, 9 (1992).
[15] A. M. Ferrenberg and R. H. Swendsen, Phys. Rev. Lett. **61**, 2635 (1988); **63**, 1658 (1989).
[16] Markov Chain Monte Carlo Simulations and Their Statistical Analysis, p. 177 (Ref. [11]).
[17] Markov Chain Monte Carlo Simulations and Their Statistical Analysis, p. 252 ff. (Ref. [11]).
[18] A. Pelissetto and E. Vicari, Phys. Rep. **368**, 549 (2002).
[19] F. Karsch and S. Stickan, Phys. Lett. B **488**, 319 (2000); N. Alves, B. A. Berg, and R. Villanova, Phys. Rev. B **43**,

5846 (1991). Note that an extra factor $3/2$ is used in the energy notation of the last article.
[20] Principles of Condensed Matter Physics, p. 484 (Ref. [3]).
[21] C. M. Fortuin and P. W. Kasteleyn, Physica (Amsterdam) **57**, 536 (1972); A. Coniglia and W. Klein, J. Phys. A **13**, 2775 (1980).
[22] S. Fortunato, J. Phys. A **36**, 4269 (2003).
[23] G. Boyd, J. Engels, F. Karsch, E. Laermann, C. Legeland, M. Lütgemeier, and B. Peterson, Nucl. Phys. **B469**, 419 (1996).
[24] A. Hasenfratz and P. Hasenfratz, Phys. Lett. B **93**, 165 (1980).
[25] J. D. Gunton and M. Droz, *Introduction to the Theory of Metastable and Unstable States* (Springer, Berlin, 1985).
[26] J. W. Cahn, Trans. Metall. Soc. AIME **242**, 166 (1968).
[27] J. W. Cahn and J. E. Hilliard, J. Chem. Phys. **28**, 258 (1958).
[28] A. Velytsky, Ph.D. thesis, Florida State University, 2004 (unpublished). On the web at http://etd.lib.fsu.edu.
[29] O. Kaczmarek, F. Karsch, F. Zantow, and P. Petreczky, Phys. Rev. D **70**, 074505 (2004); O. Kaczmarek and F. Zantow, Phys. Rev. D **71**, 114510 (2005).
[30] P. Petreczky, Nucl. Phys. B, Proc. Suppl. **140**, 78 (2005); E. Laermann and O. Philipsen, Annu. Rev. Nucl. Part. Sci. **53**, 163 (2003).
[31] J. Engels, F. Karsch, and T. Scheideler, Nucl. Phys. **B564**, 303 (2000).
[32] Y. Deng, Nucl. Phys. B, Proc. Suppl. **9**, 334 (1989); J. Engels, J. Fingberg, F. Karsch, D. Miller, and M. Weber, Phys. Lett. B **252**, 625 (1990).
[33] U. W. Heinz, AIP Conf. Proc. **739**, 163 (2004); P. F. Kolb, Acta. Phys. Hung. N.S **21**, 243 (2004); P. F. Kolb and U. W. Heinz, in *Quark Gluon Plasma 3*, edited by R. C. Hwa and X. N. Wang (World Scientific, Singapore, 2004); nucl-th/0305084.
[34] R. D. Pisarski, Phys. Rev. D **62**, 111501(R) (2000); A. Dumitru and R. Pisarski, Phys. Lett. B **504**, 282 (2001).
[35] O. Scavenius, A. Dumitru, and A. D. Jackson, Phys. Rev. Lett. **87**, 182302 (2001).